Kaon inelastic scattering and charge exchange on nuclei

C. B. Dover
Brookhaven National Laboratory, Upton, New York 11973

G. E. Walker
Physics Department, Indiana University, Bloomington, Indiana 47401

(Received 26 October 1978)

We present the results of calculations of kaon inelastic and charge exchange reactions on nuclei, based on the microscopic particle-hole shell model. Both K^+ and K^- inelastic scattering on ^{12}C are discussed for incident momenta $p_{lab} = 300$ MeV/c and 800 MeV/c. In addition, we examine the charge exchange process $^{30}Si(K^-,\bar{K}^0)^{30}Al$ at 300 MeV/c. We employ the distorted wave impulse approximation, using a transition operator constructed from free space $K^{\pm}$-nucleon amplitudes taken from analyses of two-body data. For the off-shell extrapolation of the two-body t matrix, required in the many-body problem, we use a separable form factor obtained by solving the inverse scattering problem. The inelastic scattering results are found to be insensitive to the presence of the off-shell form factor. We find that normal parity $T = 0$ and 1 states dominate the nuclear response to both K^+ and K^-. At 300 MeV/c, some qualitative differences in the inelastic scattering predictions arise from choosing different elementary amplitudes from the literature. Thus kaon-nucleus scattering may shed some light on ambiguities in the low energy free space interactions of kaons. At 800 MeV/c, there is much less uncertainty in the two-body t matrix, so we can focus our attention on nuclear structure aspects. We compare the kaons with pions, electrons, protons, and α in terms of their inelastic scattering and charge exchange properties. By emphasizing nuclear structure aspects such as the excitation of high spin states and the splitting of the $T_<$ and $T_>$ components of giant resonances, we show that kaons are very promising as a nuclear probe.

[NUCLEAR REACTIONS, NUCLEAR STRUCTURE $^{12}C(K^{\pm},K^{\pm\prime})^{12}C^*$ $p_{lab} \approx 300$–800 MeV/c; $^{30}Si(K^-, \bar{K}^0)^{30}Al^*$, $p_{lab} = 300$ MeV/c theoretical estimates based on DWIA for kaon inelastic and charge exchange $d\sigma/d\Omega$; virtues of kaons as nuclear structure probe.]

I. INTRODUCTION

One of the fundamental difficulties in the interpretation of projectile-nucleus scattering is the incomplete knowledge of the relevant nuclear structure and also the projectile-target reaction mechanism. Heretofore, the primary projectile possessing a well understood reaction mechanism has been the electron. For nuclear projectiles, particularly hadrons such as the proton and pion, there is hope that by using the new generation of intense beam current medium energy machines, such as the Clinton P. Anderson Meson Physics Facility (LAMPF) and the Indiana University Cyclotron Facility (IUCF), the appropriate reaction mechanism will simplify and the usual approximations associated with practical applications of multiple scattering theory, such as the impulse approximation,[1] will become adequate. Clearly though, because of the uncertainties in the reaction mechanism and the inherent limitations of each particle for elucidating nuclear structure, there is strong motivation to look for additional elementary nuclear probes. Such a probe would be especially welcomed if its interactions with target nuclei could be studied at existing facilities. The purpose of this paper is to indicate that a study of kaon-nucleus reactions would be an additional fruitful area of nuclear physics research. The types of experiments we discuss could be performed, for example, at the AGS at Brookhaven National Laboratory.

The K^+ and K^- differ significantly in their strong interaction with the nucleus, unlike π^+ and π^-. This difference is related to the fact that K^+ and K^- possess strangeness S, a conserved quantity in strong interactions. We have $S = +1$ for K^+ and $S = -1$ for K^-; the only baryons with $|S| = 1$ stable with respect to strong interactions have $S = -1$ (Λ and Σ).

In the energy interval $100 \leq T_K^{lab} \leq 500$ MeV, the K^+ – nucleon (K^+N) interaction is relatively weak ($\sigma_T \approx 10$ mb) and smoothly varying with energy.[2] There are no open inelastic channels below pion production threshold. The associated nuclear mean free path, $\lambda = (\rho\sigma_T)^{-1}$, is approximately 5–7 fm (see Fig. 1) so the K^+ is a *weakly* absorbed projectile capable of probing the nuclear interior. The K^+ is the only hadron exhibiting this property. Thus the K^+ – nucleus interaction should be relatively easily understood and quantitatively reliable calculations should be possible.

In contrast, the K^-N interaction is relatively

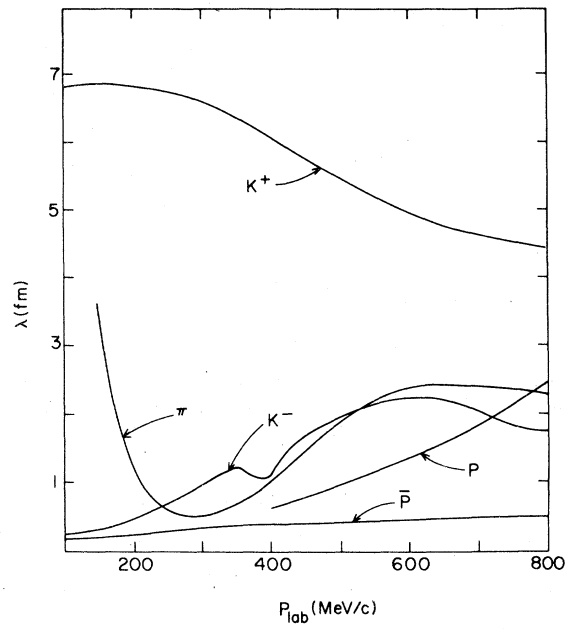

FIG. 1. Mean free path λ of various hadrons in nuclei as a function of lab momentum $p_{\rm lab}$. We use the nuclear matter estimate $\lambda = (\rho\sigma_{AV})^{-1}$, where $\rho = 0.16$ fm^{-3} is the density and $\sigma_{AV} = (\sigma_p + \sigma_n)/2$ is the average of elementary hadron-proton and hadron-neutron cross sections σ_p and σ_n. For incident protons (P), we use $\sigma_{AV}(b) = \sigma_{np} \approx 8.5/T_{\rm lab}$ (MeV), where $T_{\rm lab}$ is the lab kinetic energy. For antiprotons ($\bar{P}$), we use $\sigma_{\bar{p}n} \approx \sigma_{\bar{p}d} - \sigma_{\bar{p}p}$ and $\sigma^{\bar{P}}_{AV}$ (mb) $\approx 64.5 + 39/p_{\rm lab}$ (GeV). For K^+, we took the amplitudes of B. Martin (Ref. 18) to evaluate σ_{AV}, while for K^-, we applied the amplitudes of Gopal *et al.* (Ref. 15). We have not Fermi-averaged any of the elementary cross sections, which would tend to smooth out the rapid energy dependence of λ for pions (π) and for K^- near 400 MeV/c [the $Y^*(1520)$ resonance].

strong ($\sigma_T \gtrsim 30$ mb for $100 \leq T_K^{\rm lab} \leq 500$ MeV) and rapidly varying with energy.[2] The K^-N interaction is further complicated by the fact that there exist several reaction channels, involving final state hyperons, the $\Lambda\pi$ and $\Sigma\pi$ channels, with negative energy thresholds. Nevertheless, K^- nucleus inelastic scattering and charge exchange are important objects of study, even if one does not have great confidence in the accuracy of the theoretical calculations. As we show in Sec. III, the spectrum of excited states which dominate the nuclear response to K^- displays some intriguing features. In certain kinematical regions, one may also study how the various Y^* resonances associated with the K^-N interactions are modified in the many-body environment. Of course, the K^- is uniquely suited for the study of single strangeness exchange via ($K^-\pi^-$) and double strangeness exchange via (K^-K^+), with associated single and double hypernucleus formation, respectively.

Previous theoretical work[2-7] has stressed the utility of the K^+ for studying the nucleus. Earlier studies of K^+ inelastic scattering have used the plane wave approximation or simple collective models to study the prominent low-lying normal parity, $T = 0$ nuclear final states.[3,4,7]

In this paper we study $K^\pm$ inelastic scattering and charge exchange at $p_K^{\rm lab} = 300$ MeV/c ($T_K^{\rm lab} = 84$ MeV) and 800 MeV/c ($T_K^{\rm lab} = 447$ MeV). The predictions which we report are based on a fully microscopic calculation in the distorted wave impulse approximation, using a separable form for the off-shell kaon-nucleon transition t matrix.[8] We include s, p, and d waves in the elementary amplitude. Kaon distorted waves in the entrance and exit channel are obtained from an optical potential motivated by multiple scattering theory. The Tamm-Dancoff approximation (TDA) has been adopted to obtain the energies and wave functions for the final particle-hole (p-h) states reached via the kaon-nucleus reaction.

In Sec. II, we discuss the procedures adopted to obtain the off-shell separable form for the kaon-nucleon t matrix. We have used standard techniques, applied previously in nucleon and pion physics, involving the solution of the inverse scattering problem for separable potentials. Also in Sec. II, we briefly outline the technique used to obtain the formulas for calculating inelastic scattering and charge exchange. The procedure follows that adopted by Gupta and Walker[9] for studying pion-nucleus reactions.

The results of the calculations and the implications for studying nuclear structure with kaons are included in Sec. III. More specifically, we have carried out calculations for $^{12}C(K^\pm, K^{\pm\prime})^{12}C^*$ at $p_K^{\rm lab} = 300$ MeV/c and 800 MeV/c. We compare the results obtained with those predicted or experimentally obtained for electron, proton, and pion probes. We also have considered the charge exchange reaction $^{30}Si(K^-, \bar{K}^0)^{30}Al^*$ at 300 MeV/c. The utility of such experiments when combined with results of other probes is discussed in some detail. We have also considered the sensitivity of the results to the kaon-nucleon separable form factor and to the choice of phase shift analysis used in solving the inverse scattering problem. As summarized in Sec. III we find, for example, that at 300 MeV/c and at 800 MeV/c the results are rather insensitive to the form factor. There are situations, especially at 300 MeV/c, where different analyses of the on-shell K^+ data result in qualitatively different predictions for (K^+ nucleus) inelastic scattering.

II. PROCEDURE AND FORMULAS

A. The kaon-nucleon interaction

We have adopted a separable form for the KN interaction so that the off-shell form of the two-body t matrix can be obtained by use of standard techniques for solving the inverse scattering problem for a separable potential.[10-12] Since the details have been the subject of considerable discussion in the literature we summarize briefly here using the notation of Ref. 12. The two-body center-of-mass (c.m.) on-shell t matrix associated with channel $\alpha=\{ljt\}$ is written

$$T_\alpha(k,k;E(k))=-\frac{1}{2k}\frac{E_1+E_2}{E_1E_2}e^{i\gamma_\alpha(k)}\sin\gamma_\alpha(k), \quad (1)$$

where $E_{1,2}=(M^2_{N,K}+k^2)^{1/2}$, $E(k)=E_1+E_2$, and

$$\gamma_\alpha(k)=\delta_\alpha(k)-\frac{i}{2}\ln\eta_\alpha(k). \quad (2)$$

The fully off-shell t matrix needed for the inelastic scattering calculation is related to $T_\alpha(k,k;E(k))$ via

$$T_\alpha(k_1,k_2;E(k))=\frac{g_\alpha(k_1)g_\alpha(k_2)}{g^2_\alpha(k)}T_\alpha(k,k;E(k)). \quad (3)$$

The form factors $g_\alpha(k)$ can be obtained from the phase shifts δ_α and inelasticities η_α at all energies from the expression[12]

$$g^2_\alpha(k)=-\frac{1}{k}\frac{E_1(k)+E_2(k)}{2E_1(k)E_2(k)}\sigma_\alpha e^{-\Delta_\alpha(k)}\sin\gamma_\alpha(k), \quad (4)$$

where $\sigma_\alpha=\pm1$ and $\Delta_\alpha(k)$ is the principal value integral

$$\Delta_\alpha(k)=\frac{1}{\pi}P\int_0^\infty dp\frac{\gamma_\alpha(p)pE(p)/E_1(p)E_2(p)}{E(p)-E(k)}. \quad (5)$$

Equations (4) and (5) are appropriate if there are no bound states in the two-body system and if $\delta_L\to0$, $\eta_L\to1$ for $E\to\infty$. Since the phase shifts are known only up to some finite energy, it is necessary to join the existing phase shifts (in the general energy region where the t matrix will be used) onto some smooth cutoff form for $p\geq p_0$. If $F(p)$ is defined as

$$F(p)\equiv1, \quad p<p_0$$
$$F(p)\equiv\Lambda^2/[\Lambda^2+(p-p_0)^2], \quad p\geq p_0 \quad (6)$$

then for $p\geq p_0$, adopting the set of K^+N amplitudes in Ref. 13 and 14, here denoted BGRT$(i)D$, we define

$$\hat{\eta}(p)=1+[\eta(p)-1]F(p), \quad (7a)$$
$$\hat{\delta}(p)=\delta(p_0)F(p). \quad (7b)$$

For the K^+N form factors, we have used

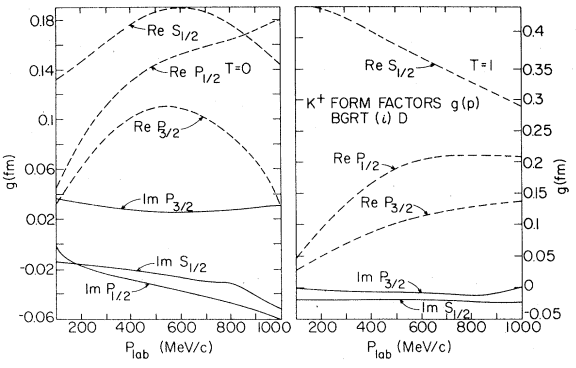

FIG. 2. Form factors $g(p)$ as a function at lab momentum p_{lab} for the K^+N system in isospin 0 (left-hand side) and isospin one (right-hand side). We plot the real (dashed lines) and imaginary (solid lines) parts of $g(p)$, as defined by Eqs. (4) and (5), for s and p waves. We have used the BGRT K^+N amplitudes of Refs. (13) and (14).

$$p_0=0.5 \text{ GeV}/c \text{ (c.m.)}, \quad \Lambda=1 \text{ GeV}/c. \quad (8)$$

The resulting form factors are shown in Fig. 2. The form factors $g(p)$ are slowly varying functions of p as one would expect from a short range interaction. Therefore one does not expect that the off-shell behavior will play a crucial role in inelastic scattering.

For the K^-N interaction we have used the phase shift solution of Gopal *et al.*[15] In this case we define

$$\hat{\eta}(p)=1+[\eta(p_0)-1]F(p), \quad (9a)$$
$$\hat{\delta}(p)=\delta(p_0)F(p), \quad (9b)$$

with

$$p_0=0.8 \text{ GeV}/c \text{ (c.m.)}, \quad \Lambda=1 \text{ GeV}/c. \quad (10)$$

Again we find that the form factors are *smoothly* varying. When first encountered, this may seem surprising since the K^-N system is really part of a multichannel problem. For the case of the πN problem, when an important open channel was available, a modified treatment of the problem was necessary[16] in order to obtain smoothly varying form factors. The difference here may be that the Y^* resonances are generally quite inelastic, and a number of them are only weakly coupled to the $\bar{K}N$ channel.[17] This is in contrast to the $\Delta(1236)$, which is an elastic resonance coupled only to the πN system. The coupling of the $\bar{K}N$ channel to $\pi\Lambda$ and $\pi\Sigma$ proceeds via $K^*(890)$ exchange. Such a short range coupling potential is in contrast to the $\pi N\to\rho N$ coupling, for instance, which proceeds by long range pion exchange. In any case, the choice of K^-N form factor has little influence on our inelastic scattering results, as we indicate later.

There are several approximations that we adopt in the next section, when the elementary amplitudes are used in the many-body problem. We have calculated cross sections in the kaon-nucleus lab system. Starting with amplitudes in the two-body c.m. system, we first transform to the two-body lab system. We now assume that the remaining $A-1$ spectator nucleons are also at rest in the lab; the two-body and many-body lab systems then are the same. Thus only lab energies and lab two-body amplitudes enter our calculation. We have also consistently used two-body lab amplitudes in our construction of the kaon optical potential. An alternative procedure is to work in the kaon-nucleus c.m. system. An angle transformation[19] is then necessary to transform from two-body to many-body c.m. systems. This transformation must also be applied consistently to the construction of the optical potential. For off-shell amplitudes, this transformation is not unique, but one version of it has been found to produce significant effects at large angles in medium energy pion-nucleus scattering,[19] where the elementary p-wave interaction dominates. For K^+ – nucleus scattering, on the other hand, the s-wave interaction dominates completely for $p_{\rm lab} \leq 500$ MeV/c and remains the most important partial wave up to about 800 MeV/c. Thus the angle transformation should not affect the results very much in the region below 800 MeV/c and for the region of small angles of interest here (later we show that even for high spin states, the inelastic cross sections at 800 MeV/c peak inside $\Theta_{\rm lab} \approx 30°$).

B. Kaon-nucleus inelastic scattering and charge exchange

The procedure adopted here follows that used in Ref. 9. The distorted wave impulse approximation (DWIA), the separable kaon-nucleon off-shell t matrix discussed in Sec. IIA and the TDA for the nuclear final particle-hole states have been employed. The lab differential cross section for inelastic scattering from an initial state a to a final nuclear state b is given by

$$\frac{d\sigma_{ab}}{d\Omega} = \frac{E_K(p_f)p_f}{E_K(p_i)p_i} \left| F_{ba}(p_f, p_i) \right|^2 , \tag{11}$$

where $E_K(p_{i,f}) = (M_K{}^2 + p_{i,f}{}^2)^{1/2}$, p_i and p_f being the initial and final kaon lab momenta, respectively. Assuming the transition operator can be written as a sum of single kaon-nucleon lab amplitudes f_{E_i}, normalized so that $(d\sigma/d\Omega)^{\rm lab}_{KN} = |f_{E_i}|^2$, we can write F_{ba} in momentum space as

$$F_{ba}(\vec{\rm p}_f \vec{\rm p}_i) = \sum_{j=1}^{A} \int d\vec{\rm p}\, d\vec{\rm p}'\, d\vec{\rm k}_1 \ldots d\vec{\rm k}_A \Phi_b^+(\vec{\rm k}_1, \vec{\rm k}_2, \ldots, \vec{\rm k}_j \ldots \vec{\rm k}_A) \times \chi^+_{E_f I_f}(\vec{\rm p}_f, \vec{\rm p}') f^j_{E_i}(\vec{\rm p}', \vec{\rm p}) \chi_{E_i I_i}(\vec{\rm p}_i, \vec{\rm p}) \Phi_a(\vec{\rm k}_1, \vec{\rm k}_2, \ldots \vec{\rm k}'_j = \vec{\rm k}_j - \vec{\rm p} + \vec{\rm p}', \ldots \vec{\rm k}_A) , \tag{12}$$

where $\chi_{E_i I_i}$ ($\chi_{E_f I_f}$) is the initial (final) kaon distorted wave including the isospin variable I_i (I_f) and the nuclear many-body states are denoted by Φ. Making use of the fact that $f^j_{E_i}$ is a single nucleon operator, and assuming that the ground state of the target nucleus is a closed shell and the excited nuclear states are p-h states treated in the TDA approximation, we can reduce Eq. (12) to

$$\sum_{l_p, l_h, j_p, j_h} \alpha^{l_h l_p}_{j_h j_p} \sum_{j_{zh}, j_{zp}, t_{zh}, t_{zp}} (-1)^{j_h - j_{zh}} (j_p j_{zp} j_h - j_{zh} | j_p j_h J J_z) (-1)^{1/2 - t_{zh}} \times (\tfrac{1}{2} t_{zp} \tfrac{1}{2} - t_{zh} | \tfrac{1}{2}\tfrac{1}{2} T T_z) \cdot \int d\vec{\rm p}\, d\vec{\rm p}'\, d\vec{\rm k}_j \phi_{l_p j_p}(k_j) \chi^+_{E_f I_f}(\vec{\rm p}_f, \vec{\rm p}') \times f_E(\vec{\rm p}', \vec{\rm p}) \chi_{E_i I_i}(\vec{\rm p}_i, \vec{\rm p}) \phi_{l_h j_h}(\vec{\rm k}_j - \vec{\rm p} + \vec{\rm p}') . \tag{13}$$

In Eq. (13), the $\alpha^{l_h l_p}_{j_h j_p}$ are the pure particle-hole admixture amplitudes in the TDA configuration mixed p-h state of spin J and the $\phi_\alpha(k)$ are the Fourier transforms of the single nucleon orbitals ($\alpha \equiv l_\alpha j_\alpha j_{z\alpha} t_{z\alpha}$), $\phi(\vec{\rm k}_j) \equiv (2\pi)^{-3/2} \int e^{-i\vec{\rm k}_j \cdot \vec{\rm r}_j} \phi(\vec{\rm r}_j) d\vec{\rm r}_j$. We have made a partial wave decomposition of the momentum space kaon distorted waves. As in Ref. 9, we have expanded the configuration space kaon wave functions, $\chi^l_E(p_i, r_k)$ in terms of spherical Bessel functions $j_l(k_n r_k)$ where the k_n have been chosen so that $j_0(k_n r_k)$ vanishes at the radius $R = 12$ fm. After taking the Fourier transform, one obtains

$$\chi^l_E(p_i, k) = \sum_n a_{nl}(p_i) \frac{\pi}{2k^2} \delta(k_n - k) . \tag{14}$$

Finally using standard techniques for angular momentum recoupling, and assuming a separable form for the elementary transition operator, one can write the square of the transition amplitude for going from a closed shell ground state to a configuration mixed p-h state of spin J as[9]

$$|F_{J0}(p_f,p_i)|^2 = \frac{1}{2(2\pi)^4}\sum_{J_z}\Big|\sum_{l_p l_h j_p j_h}\alpha^{l_p l_h}_{j_p j_h} M^{J J_z}_{l_p l_h j_p j_h}\Big|^2, \quad (15)$$

where

$$M^{J J_z}_{l_p l_h j_p j_h} = \sum_i a^*_{n l_a} a_{n' l_b}\,\alpha\beta\gamma(N+\hat{N}), \quad (15a)$$

$$\alpha = \begin{pmatrix} l & l_3 & l_b \\ 0 & 0 & 0 \end{pmatrix}\begin{pmatrix} l & l_4 & l_a \\ 0 & 0 & 0 \end{pmatrix}\hat{l}\hat{l}_4(\hat{l}_a\hat{l}_b\hat{l}_p\hat{l}_h\hat{j}_p\hat{j}_h J)^{1/2} i^{l_3-l_4}(-)^l, \quad (15b)$$

$$\beta = (-)^{m_b}\begin{pmatrix} J & l_a & l_b \\ -J_z & -m_a & m_b \end{pmatrix} Y_{l_b m_b}(\Omega_{p_f}) Y^*_{l_a m_a}(\Omega_{p_i}), \quad (15c)$$

$$\gamma = \int_0^\infty r^2 dr\, R_{l_h}(r) R_{l_p}(r) j_{l_3}(k_{n'} r) j_{l_4}(k_n r), \quad (15d)$$

$$N = (-)^{j_h+1/2}\begin{pmatrix} J & l_3 & l_4 \\ 0 & 0 & 0 \end{pmatrix}\begin{pmatrix} l_p & l_h & J \\ 0 & 0 & 0 \end{pmatrix}\begin{Bmatrix} l_p & j_p & \frac{1}{2} \\ j_h & l_h & J \end{Bmatrix}\begin{Bmatrix} J & l_a & l_b \\ l & l_3 & l_4 \end{Bmatrix} \times\left(A^{\Delta S=0}_{\Delta T=0} + B^{\Delta S=0}_{\Delta T=1}\right), \quad (15e)$$

$$\hat{N} = \sqrt{6}\sum_{\bar{J}}\begin{pmatrix} \bar{J} & l_3 & l_4 \\ 0 & 0 & 0 \end{pmatrix}\begin{pmatrix} l_p & l_h & \bar{J} \\ 0 & 0 & 0 \end{pmatrix} \times\begin{Bmatrix} l_p & \frac{1}{2} & j_p \\ l_h & \frac{1}{2} & j_h \\ \bar{J} & 1 & J \end{Bmatrix}\begin{Bmatrix} l & l_4 & l_a \\ l & l_3 & l_b \\ 1 & \bar{J} & J \end{Bmatrix} \times\hat{\bar{J}}\hat{l}^{1/2}(-)^{l_b}\left(C^{\Delta S=1}_{\Delta T=0} + D^{\Delta S=1}_{\Delta T=1}\right), \quad (15f)$$

where $i=\{l, l_3, l_4, l_a, l_b, n, n', m_a, m_b\}$ and $\hat{l}\equiv 2l+1$. In Eqs. (15a)–(15f) the factor β contains the angular dependence and γ contains the radial overlap integrals. The particle and hole radial functions $R(r)$ are normalized so that $\int_0^\infty r^2R^2(r)dr=1$. The factors N and $\hat{N}$ contain the nonspin-flip ($\Delta S=0$) and spin-flip ($\Delta S=1$) contributions, respectively. The transition amplitudes A, B, C, D are given by

$$A^{\Delta S=0}_{\Delta T=0} = l(f^0_{l-}+3f^1_{l-}) + (l+1)(f^0_{l+}+3f^1_{l+}), \quad (16a)$$

$$B^{\Delta S=0}_{\Delta T=1} = l(f^0_{l-}-f^1_{l-}) + (l+1)(f^0_{l+}-f^1_{l+}), \quad (16b)$$

$$C^{\Delta S=1}_{\Delta T=0} = [l(l+1)]^{1/2}(f^0_{l+}-f^0_{l-}+3f^1_{l+}-3f^1_{l-}), \quad (16c)$$

$$D^{\Delta S=1}_{\Delta T=1}[l(l+1)]^{1/2}(f^0_{l+}-f^0_{l-}+f^1_{l-}-f^1_{l+}). \quad (16d)$$

The quantities $f^I_{l\pm}$ are off-shell *lab* K^+N amplitudes for isospin I and $J=l\pm\frac{1}{2}$. We obtain these from the corresponding on-shell c.m. amplitudes $f^{I,\mathrm{c.m.}}_{l\pm}$ via

$$f^I_{l\pm} = \frac{p_{\mathrm{lab}}}{k}\frac{g^I_{l\pm}(k_{n'})g^I_{l\pm}(k_n)}{[g^I_{l\pm}(k)]^2} f^{I,\mathrm{c.m.}}_{l\pm}, \quad (17)$$

where p_{lab} and k are the two-body lab and c.m. incident momenta, related by $p_{\mathrm{lab}}/k=[1+m_K^2/m_N^2+2(m_K^2+p^2_{\mathrm{lab}})^{1/2}/m_N]^{1/2}$ and the form factors $g^I_{l\pm}(p)=g_\alpha(p)$ are obtained from Eq. (4). The off-shell momenta $k_{n'}$ and k_n are defined by Eq. (14). It would be more consistent to employ lab form factors $g(p)$ obtained from the appropriate lab phase shifts. However, the off-shell extrapolation does not influence our results much in any case. The c.m. partial wave amplitudes $f^{I,\mathrm{c.m.}}_{l\pm}$ are related to the two-body c.m. cross section $(d\sigma/d\Omega)_{K^\pm N}$ by

$$d\sigma/d\Omega = |f^{\mathrm{c.m.}}|^2,$$

$$f^{\mathrm{c.m.}} = \sum_{l=0}^\infty[(l+1)f^{\mathrm{c.m.}}_{l+} + lf^{\mathrm{c.m.}}_{l-}], \quad (18)$$

$$f^{\mathrm{c.m.}}_{l\pm} = \frac{1}{k}e^{i\gamma_{l\pm}}\sin\gamma_{l\pm},$$

where $\gamma_{l\pm}$ is given by Eq. (2). In order to use Eq. (15) for kaon charge exchange $(K^-, \bar{K}^0)$, we simply set $A=C=0$, since $\Delta T=1$, and multiply the cross section by a factor of two.

It is particularly instructive to focus attention on A, B, C, and D in Eq. (15). By examining these terms (which are classified by their spin and isospin flip properties; as examples, A flips neither spin or isospin and D flips both) one can easily predict the spin and isospin character of the strongly excited nuclear final states obtained in kaon inelastic scattering and charge exchange. Terms A–D are studied in detail as a function of energy for both K^+ and K^- in the next section.

The optical potentials adopted for calculating kaon distorted waves were obtained by using standard approximations in conjunction with multiple scattering theory. A modified version of the program PIRK[20] was used for the actual distorted wave calculations. For the 300 MeV/c kaon distorted waves on ^{12}C, ^{30}Si, and ^{30}Al, a Kisslinger[21] form for the optical potential $V(r)$ was chosen,

$$-2E_K V(r) = p^2_{\mathrm{lab}} b_0\rho(r) - b_1\nabla\cdot\rho(r)\nabla, \quad (19)$$

where $\rho(r)$ is normalized to the total number of nucleons A, and b_0 and b_1 are in units of fm^3 and are related to the spin-isospin averaged s and p-wave kaon-nucleon scattering amplitudes by

$$p^2_{\mathrm{lab}} b_l = 4\pi(f^{AV}_l)_{\mathrm{lab}} = \frac{4\pi p_{\mathrm{lab}}}{k}(f^{AV}_l)_{\mathrm{c.m.}}, \quad (20)$$

where

$$(f^{AV}_l)_{\mathrm{c.m.}} = \frac{1}{A}(Zf^{\mathrm{c.m.}}_{K^+p} + Nf^{\mathrm{c.m.}}_{K^+n}) = \frac{1}{2A}[Z\Sigma_1 + (N-Z)\Sigma_2], \quad (21)$$

with

$$\Sigma_1 = \sum_{I=0,1} (2I+1)[(l+1)f_{l+}^{I,\text{c.m.}} + lf_{l-}^{I,\text{c.m.}}],$$
$$\Sigma_2 = \sum_{I=0,1} [(l+1)f_{l+}^{I,\text{c.m.}} + lf_{l-}^{I,\text{c.m.}}]. \quad (22)$$

For K^-N, we also use Eqs. (21) and (22), but with N replaced by Z and vice versa. For $K^+ + {}^{12}\text{C}$, using the amplitudes of Martin *et al.*,[18] we obtain

$$\left.\begin{aligned} b_0 &= -2.04 + 0.62i \\ b_1 &= 0.14 + 0.046i \end{aligned}\right\} \text{for } p_{\text{lab}} = 300 \text{ MeV}/c \quad (23)$$

and

$$\left.\begin{aligned} b_0 &= -0.26 + 0.20i \\ b_1 &= 0.077 + 0.14i \end{aligned}\right\} \text{for } p_{\text{lab}} = 800 \text{ MeV}/c, \quad (24)$$

while in contrast, using the K^+N amplitudes of BGRT$(i)D$ of Ref. 13, one obtains

$$\left.\begin{aligned} b_0 &= -1.99 + 0.56i \\ b_1 &= 0.19 + 0.058i \end{aligned}\right\} \text{for } p_{\text{lab}} = 300 \text{ MeV}/c \quad (25)$$

and

$$\left.\begin{aligned} b_0 &= -0.26 + 0.17i \\ b_1 &= 0.10 + 0.19i \end{aligned}\right\} \text{for } p_{\text{lab}} = 800 \text{ MeV}/c. \quad (26)$$

For $K^- + {}^{12}\text{C}$ at $p_{\text{lab}} = 300$ MeV/c, using the amplitudes of Gopal *et al.*,[15] the results are

$$b_0 = 1.41 + 3.86i,$$
$$b_1 = -0.088 + 0.42i \quad (27)$$

and for ${}^{30}\text{Si}(K^-, \bar{K}^0){}^{30}\text{Al}$, using the amplitudes of Ref. 15, we have

$$\begin{aligned} b_0 &= 1.44 + 3.80i \text{ for } K^- \text{ at } 300 \text{ MeV}/c, \\ b_0 &= 2.11 + 6.11i \text{ for } \bar{K}^0 \text{ at } 275 \text{ MeV}/c, \\ b_1 &= -0.12 + 0.43i \text{ for } K^- \text{ at } 300 \text{ MeV}/c, \\ b_1 &= -0.20 + 0.55i \text{ for } \bar{K}^0 \text{ at } 275 \text{ MeV}/c. \end{aligned} \quad (28)$$

Near 800 MeV/c, the K^-N amplitudes are rapidly varying and d waves are non-negligible. It is thus necessary to Fermi-average the amplitudes of Ref. 15. We use a local optical potential of the form

$$-2E_K V(r) = p_{\text{lab}}^2 b_0 \rho(r), \quad (29)$$

where for $K^- + {}^{12}\text{C}$ at 800 MeV/c, the Fermi-averaged total amplitude is

$$b_0 = 0.51 + 0.87i \text{ fm}^3. \quad (30)$$

We have used both harmonic oscillator (modified Gaussian) and Saxon-Woods form factors for the ground state density, $\rho(r)$, appearing in the elastic scattering optical potential. For the results presented in this paper we have used the following densities for the $K^\pm + {}^{12}\text{C}$ calculations at 300 MeV/c:

$$\rho(r) = \frac{\rho_0}{(1 + e^{(r-R)/a})}, \quad a = 0.56 \text{ fm}, \quad R = 1.722 \text{ fm}. \quad (31)$$

For the ${}^{30}\text{Si}$ and ${}^{30}\text{Al}$ densities, we took

$$\rho(r) = \rho_0/(1 + e^{(r-R)/a}), \quad a = 0.52 \text{ fm}, \quad R = 3.18 \text{ fm}. \quad (32)$$

In conjunction with the 800 MeV/c calculations, we have used the ${}^{12}\text{C}$ density

$$\rho(r) = \rho_0 \left(1 + \frac{(Z-2)r^2}{3R^2}\right) e^{-r^2/R^2}, \quad R = 1.68 \text{ fm}. \quad (33)$$

The p-h wave functions were obtained using the Tamm-Dancoff approximation and a Serber-Yukawa residual interaction that has been previously utilized to obtain wave functions for studying inelastic electron,[22] pion,[9] and proton[23]-nucleus scattering. Harmonic oscillator orbitals were used for the single nucleon wave functions with oscillator parameters, $b = (\hbar/m\omega)^{1/2} = 1.64$ fm for ${}^{12}\text{C}$ and 1.8 fm for ${}^{30}\text{Al}$. For ${}^{12}\text{C}$, the single particle and hole energies are those utilized in Ref. 22. For ${}^{12}\text{C}$, we include $2s$-$1d$ and $1p_{1/2}$ particle shells and $1s_{1/2}$ and $1p_{3/2}$ hole shells. After configuration mixing, a low lying $J = 1^-$, $T = S = 0$ essentially spurious state was eliminated from further consideration.

We assumed that the ${}^{30}\text{Si}$ ground state consists of two $2s_{1/2}$ neutrons, coupled to $J = 0$, $T = 1$, outside of a doubly closed $1d_{5/2}$ core. The $T = 2$, $T_z = -2$ final states reached via the reaction ${}^{30}\text{Si}(K^-, \bar{K}^0){}^{30}\text{Al}$ are assumed to consist of $1d_{5/2}$, $1p_{3/2}$, and $1p_{1/2}$ proton holes and $1d_{3/2}$, $2p$-$1f$ neutron particles. The single neutron particle energies were obtained by using ${}^{31}\text{Si}_{\text{g.s.}} - m_n - {}^{30}\text{Si}_{\text{g.s.}} = -6.59$ MeV (Ref. 24) for the $1d_{3/2}$ single particle energy, as well as the excitation energy *difference* between the $1d_{3/2}$ level and the $1f$-$2p$ single neutron levels for ${}^{32}\text{S}$ as listed in Ref. 22 and originally taken from Ref. 25. Thus the most unbound single particle level considered was the $1f_{5/2}$ which was taken to have a single particle energy of 2.31 MeV. The proton-hole configuration energies were obtained by using ${}^{29}\text{Al}_{\text{g.s.}} + m_p - {}^{30}\text{Si}_{\text{g.s.}} = 13.51$ MeV for the $1d_{5/2}$ proton hole energy and the binding energy difference between the $1d_{5/2}$ level and the deeper bound $1p_{3/2}$ and $1p_{1/2}$ levels for ${}^{28}\text{Si}$ as listed in Ref. 22 and obtained originally from Ref. 26. The admixture amplitudes and energies for the ${}^{12}\text{C}$ and ${}^{30}\text{Al}$ wave functions are available from the authors upon request. The excitation energies listed for

^{30}Al in the next section are relative to the ground state of ^{30}Si. The lowest state, calculated to be a 3^+, has been set equal to the $^{30}\mathrm{Al}_{g.s.} - {}^{30}\mathrm{Si}_{g.s.}$ experimental energy difference of 8.54 MeV.[24] This necessitated lowering all of the calculated excitation energies for ^{30}Al by 0.6 MeV.

III. RESULTS AND DISCUSSION

As mentioned in the previous section, the functions $A^{\Delta S=0}_{\Delta T=0}$, $B^{\Delta S=0}_{\Delta T=1}$, $C^{\Delta S=1}_{\Delta T=0}$, and $D^{\Delta S=1}_{\Delta T=1}$, given by Eqs. (16a)–(16d), are very useful for predicting the spin and isospin structure of the final states strongly excited via a single nucleon transition operator operating on the ground state wave function. In the special case where the nuclear ground state has $J=L=S=T=0$, as in an $N=Z$ double major closed shell nucleus, the subscripts and superscripts on A–D immediately yield the spin and isospin of the final nuclear excited state reached by that particular part of the transition operator.

In Figs. 3 and 4, we show the functions $|A|^2$ – $|D|^2$ for $l=0$ and 1 for several different choices of the elementary K^+N amplitudes. First consider the situation near 300 MeV/c. In this region the $|A|^2$, $l=0$ term completely dominates. While the different solutions yield significant differences, for example, in the ratios of the $l=1$ $|B|^2$ to $|D|^2$, all agree that the nonspin flip, nonisospin flip term $|A|^2$ should dominate. Thus $T=0$ normal parity states would be predicted to dominate the $K^+ + {}^{12}$C inelastic scattering at 300 MeV/c.

In Fig. 5, the functions $|A|^2$ to $|D|^2$ are shown for $l=0$, 1, 2 for the K^-N amplitudes of Gopal *et al.*[15] Once again in the region near 300 MeV/c, the $l=0$ nonspin nonisospin flip term $|A|^2$ dominates. Thus, from these considerations, one would predict that near $p^{\mathrm{lab}}_{K^\pm}=300$ MeV/c, the K^+ and K^- inelastic spectrum on ^{12}C would look quite similar, with normal parity $T=0$ states being most strongly excited for *all* values of *momentum transfer*.

If we consider K^- charge exchange, then the terms $|A|^2$ and $|C|^2$ vanish and thus it is of interest to investigate the relative size of $|B|^2$ and $|D|^2$ near 300 MeV/c. From Figs. 3 and 4, one finds that the $l=0$, $|B|^2$ term dominates, with the $l=1$, $|B|^2$ term being the next most important.

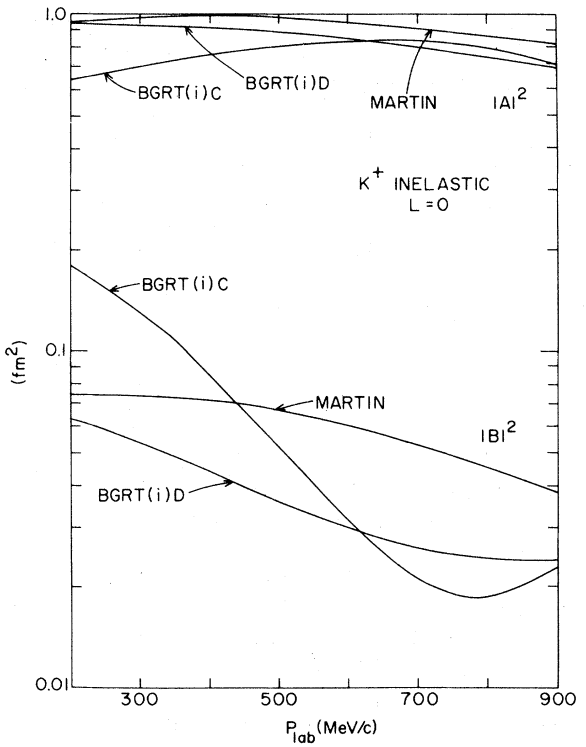

FIG. 3. The inelastic scattering functions $|A^{\Delta S=0}_{\Delta T=0}|^2$ and $|B^{\Delta S=0}_{\Delta T=1}|^2$ corresponding to the s-wave part of the K^+N amplitude. We use the definitions of Eqs. (16a) and (16b), with the two body c.m. amplitudes $f^{I}_{l\pm}{}^{\mathrm{c.m.}}$, replacing the lab amplitudes for convenience. Three models for the elementary interaction, labeled MARTIN (Ref. 18), BGRT (*i*)*C* [soln *C* of Ref. 13 for isospin zero, soln (*i*) of Ref. 14 for isospin one] and BGRT (*i*) *D* (soln *D* of Ref. 13 for $I=0$) are shown. No off-shell form factors are included here or in Figs. 4 and 5, i.e., $g(p)=1$.

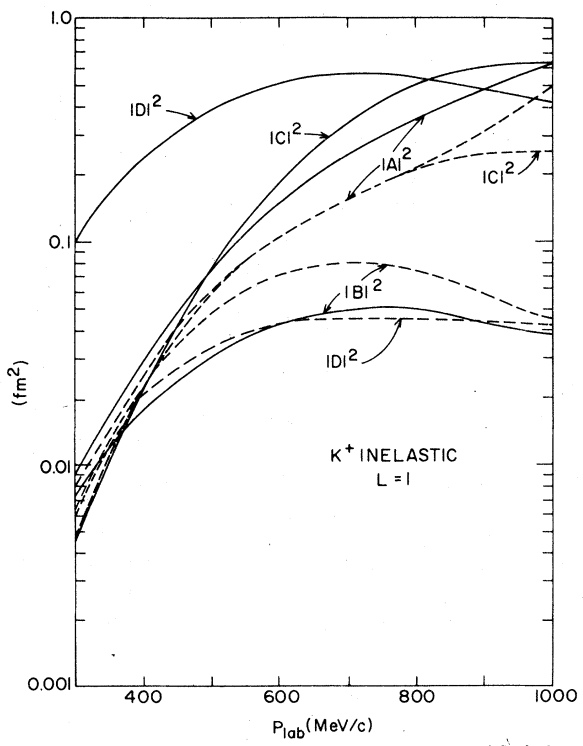

FIG. 4. The inelastic scattering functions $|A^{\Delta S=0}_{\Delta T=0}|^2$, $|B^{\Delta S=0}_{\Delta T=1}|^2$, $|C^{\Delta S=1}_{\Delta T=0}|^2$, and $|D^{\Delta S=1}_{\Delta T=1}|^2$ corresponding to the p-wave part of the K^+N amplitude. The solid curves correspond to model BGRT (*i*) *D* of Refs. 13, 14 while the dashed curves follow from the amplitudes of Martin (Ref. 18).

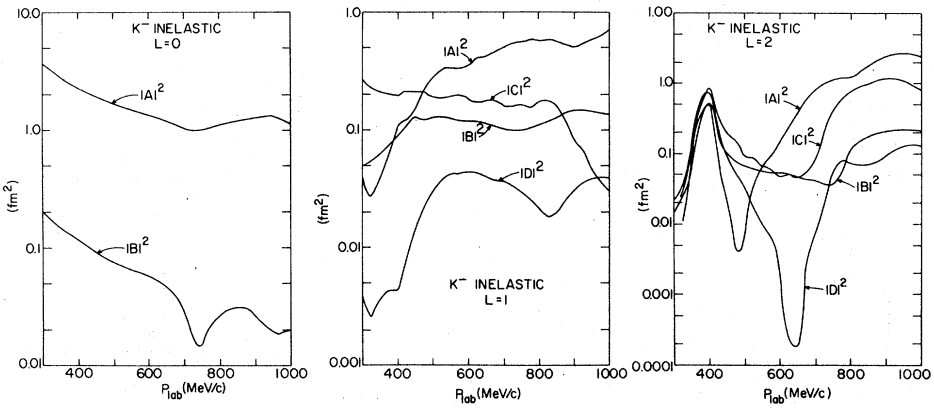

FIG. 5. The inelastic scattering functions $|A|^2$, $|B|^2$, $|C|^2$, and $|D|^2$ of Eqs. (16a)–(16d) for the s, p and d waves of the K^-N system, using the amplitudes of Gopal *et al.* (Ref. 15). The amplitudes have not been Fermi-averaged; this would tend to wash out some of the rapid energy dependences, for instance the peak near the $Y^*(1520)$ resonance at 400 MeV/c in $L=2$.

Since the $|B|^2$ term dominates, one predicts that the normal parity ($\Delta S = 0$) excited states of ^{30}Al will dominate the reaction $^{30}\mathrm{Si}(K^-, \bar{K}^0)^{30}\mathrm{Al}$ near 300 MeV/c for all values of momentum transfer. We shall discuss the 800 MeV/c predictions later in this section.

Before presenting the actual inelastic scattering and charge exchange results it may be useful to review briefly the kinds of states seen or predicted for inelastic scattering of medium energy electrons, pions, and protons.

For electrons at small angles and small momentum transfers, the normal parity $T = 0$ states (with the important exception of the $T = 1$ giant dipole and dipole spin-flip resonances) dominate the spectrum.[27] At large momentum transfers (which implies large angles here) the transverse form factor, which is dominated by the isovector magnetic moment, is the most important part of the inelastic electron scattering cross section, so that $T = 1$ non-normal parity states are most strongly excited.[22] Since one is working at large momentum transfer, the states are of relatively high spin, for example a 4^-, $T = 0$ state dominates the $^{12}\mathrm{C}(e, e')^{12}\mathrm{C}^*$ spectrum.[28]

Pion inelastic scattering results are sparse. However, the preliminary results are in agreement with predictions.[29,9] Here we discuss only the predictions. Near the (3, 3) resonance, one finds that at low excitation energy the normal parity $T = 0$ "collective" states are predicted[29] to be strongly excited. However, above 10 MeV nuclear excitation, there is a strong preference for $T = 0$ non-normal parity states to be excited (again with the exception of the giant dipole resonance).[9] In particular in (π, π') on ^{12}C and ^{16}O one predicts[30,29] that in the region of momentum transfer ~250–350 MeV/c, a high spin non-normal parity (4^-, $T = 0$) state dominates the spectrum in contrast to the $T = 1$ states for the electron. It can be easily shown, by examining the symmetries of the vector addition coefficients in Eq. (15), that neither the pion nor the kaon can excite 0^- states in a parity conserving process starting from a 0^+ ground state. Detection of the excitation of such states via mesons (perhaps by looking at their subsequent γ decay in favorable cases) could provide useful information on parity violating processes in medium energy meson-nucleus inelastic scattering. Finally, for the pion, Gupta and Walker[9] have shown that the importance of spin-flip nonisospin-flip pion inelastic excitations can be understood by looking at the $|B|^2$, $|C|^2$, and $|D|^2$ terms for pions and noting that the ($j = \frac{3}{2}$, $t = \frac{3}{2}$) partial wave dominates intermediate energy pion-nucleon scattering.

There has been considerable theoretical and experimental work on medium energy inelastic proton scattering. As with other probes, at low excitation energy and low momentum transfer, normal parity $T = 0$ states dominate the excitation spectrum. However, at higher momentum transfer ($\gtrsim$ 300 MeV/c) and between 10–20 MeV excitation in ^{12}C and ^{16}O, a non-normal parity 4^-, $T = 1$ state is most strongly excited via the *direct* term in the transition matrix.[23] This is the same state seen in inelastic electron scattering at high momentum transfer. In general, in both inelastic electron scattering and for the direct term in inelastic proton scattering, one predicts correctly[31] that high spin non-normal parity "stretched" configurations dominate at large momentum transfer. The exchange term in inelastic proton scattering results in the excitation of high spin $T = 0$ normal and non-normal parity states in such light nuclei as ^{16}O and ^{28}Si.[23] These transitions may be less

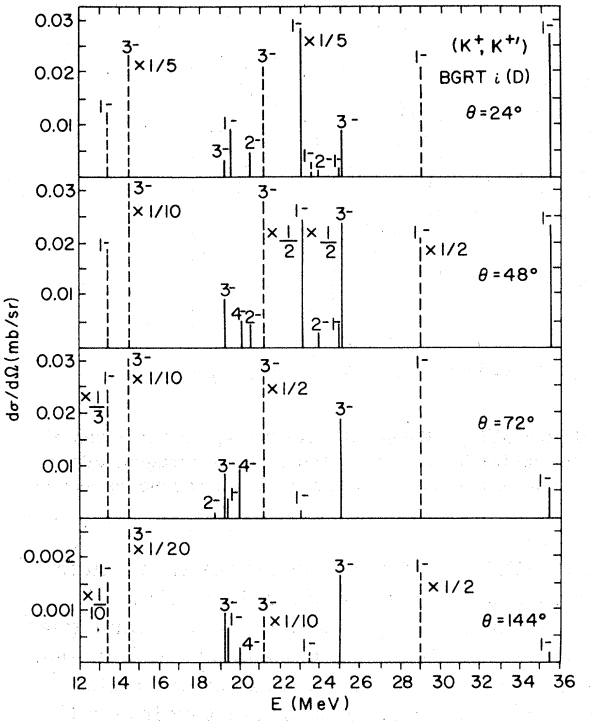

FIG. 6. Differential lab cross sections for K^+ inelastic scattering on ^{12}C at $p_{lab} = 300$ MeV/c, for various choices of lab angle θ. The excitation energy E is measured with respect to the ground state of ^{12}C. The dashed lines correspond to isospin zero ($T=0$) final states, while the solid lines are for $T=1$ states. The final states are configuration-mixed particle-hole states of negative parity, as described in the text. Final states with very small cross sections are not plotted. The cross sections for several strong states have been multiplied by numerical factors of $\frac{1}{2}$ to $\frac{1}{20}$ as indicated. We have used the K^+N amplitudes BGRT $(i)D$ of Refs. 13, 14. The bar graphs plotted here represent the cross sections to diagonalized particle-hole states; we have omitted the widths and energy shifts of these states which arise from nucleon emission or from mixing with more complicated states $(2p\text{-}2h)$.

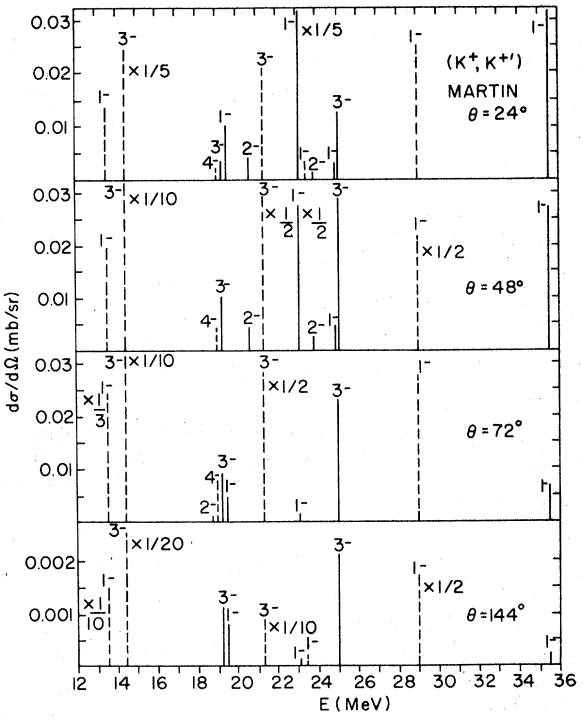

FIG. 7. Differential lab cross sections for K^+ inelastic scattering on ^{12}C at $p_{lab} = 300$ MeV/c. The kinematics and final states are the same as Fig. 6, except that we use the K^+N amplitudes of Martin (Ref. 18). No off-shell form factor was included here $[g(p)=1]$, or in any of the other calculations in this paper which employ the Martin amplitude for K^+N.

reliably predicted using standard theoretical techniques.

With this brief summary, we now turn to the actual $^{12}C(K^+,K^{+\prime})^{12}C^*$ theoretical calculations for $p_{lab} = 300$ MeV/c. The results are shown for several angles in Fig. 6, using the BGRT$(i)D$ amplitudes for the elementary K^+N interaction. In this and following calculations the reader should bear in mind that there are many p-h odd parity states in the excitation energy interval considered (and we have calculated the inelastic scattering cross section for each of them) but only those states shown in the figures have appreciable inelastic cross section. As suggested by examining Figs. 3 and 4, $T=0$ normal parity states (1^-, 3^-), dominate the spectrum shown with high spin (3^-) states being relatively more important at higher momentum transfers. The two exceptions to this rule are the giant dipole 1^-, $T=1$ state between 23 and 24 MeV and a 3^-, $T=0$ state near 25 MeV. We note that the excitation spectrum for the same reaction using the Martin amplitudes with form factors $g(p)=1$ predicts the same states to be strongly excited. This is shown in Fig. 7. The main difference between the two sets of amplitudes occurs in the predictions for the $T=0$, 1 high spin non-normal parity states as shown in Fig. 8. The Martin (BGRT) amplitudes result in more than an order of magnitude enhancement of the 4^-, $T=0$ ($T=1$) state over the $T=1$ ($T=0$) state. Although the difference in the prediction for these states is dramatic, relative to other states, the 4^- states are not supposed to be strongly excited so that seeing them in inelastic scattering may be difficult. One way to identify the 4^- state in the neighborhood of 19 MeV is to study (K^+,K^0) on ^{12}C where only $T=1$ states can be excited. In the event the 4^-, $T=0$ state is appreciably excited, as predicted by the Martin amplitudes, the peak near 19 MeV in the region of 60° should be significantly de-

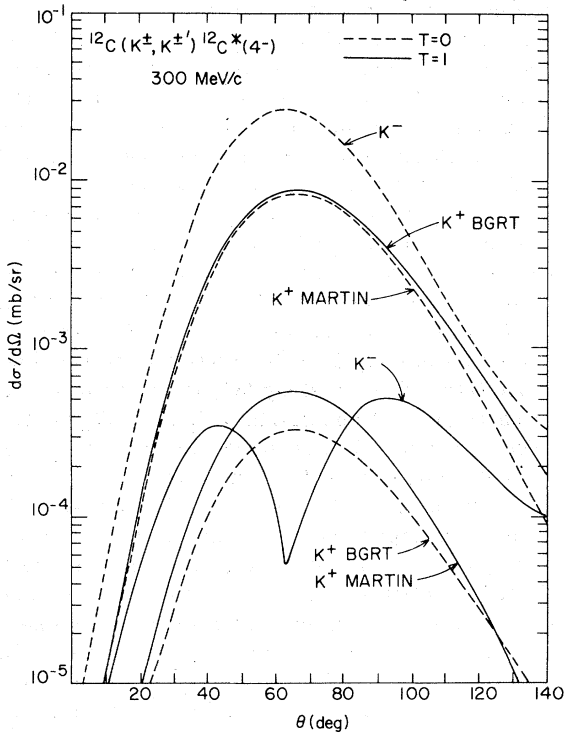

FIG. 8. Angular distributions for the $K^{\pm}$ inelastic excitation at 300 MeV/c of the 4^-, $T=0$ and 1 states at 19 and 20 MeV in ^{12}C, respectively. In our model, these states are pure $d_{5/2}p_{3/2}^{-1}$ particle-hole configurations. The dashed and solid curves refer to the $T=0$ and 1 final states, respectively. The K^- amplitudes are from Ref. 15; the K^+ amplitudes are either from Ref. 18, labeled MARTIN: or solution $(i)D$ of Refs. 13,14, labeled BGRT. Note the large difference between the predictions of BGRT and MARTIN amplitudes for excitation of the 4^- states with K^+.

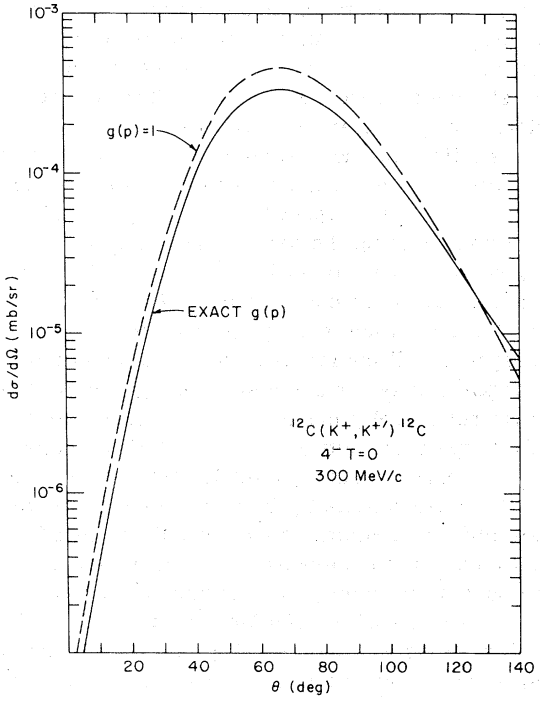

FIG. 9. Effect of the off-shell extrapolation of the K^+N amplitude on differential cross sections for the 4^-, $T=0$ state in ^{12}C at 300 MeV/c. The solid curve represents a calculation which includes the exact off-shell form factor $g(p)$ of Eqs. (3) and (4). The dashed curve corresponds to the approximation $g(p)=1$ i.e., replacing the off-shell amplitude by its on-shell version [BGRT $(i)D$ of Refs. 13, 14]. The small changes shown here also are characteristic of other final states.

creased in the charge exchange reaction (relative to other $T=1$ complex peaks such as that associated with the 1^-, $T=1$ dipole state).

The effect of setting the form factor $g(p)$ equal to one is usually quite small. A representative result is shown in Fig. 9. In general, the cross sections change by less than 50%, so that, for example, the difference in the predictions for non-normal parity states for the different phase shift solutions, BGRT$(i)D$ and Martin, is an order of magnitude greater than that due to form factor effects.

The result that normal parity $T=0$ states dominate the spectrum for K^+ inelastic scattering over a wide region of momentum transfer is very important for nuclear structure studies, especially because the K^+ nucleus interaction is weak and slowly varying with energy and thus the reaction mechanism should be reliably understood. For low excitation energy the K^+ results should be compared with those obtained using the other reliable probe, the electron, for such states as the 2^+, $T=0$ and 3^-, $T=0$ states below 10 MeV in ^{12}C. Previously, it has been necessary to at least use the RPA to get satisfactory agreement between theory and experiment for electroexcitation of these states. The *same* wave functions which yield excellent results for electroexcitation should also yield very good results for K^+ inelastic scattering. If this is not the case, then something may be wrong with our understanding of the reaction mechanism for one or both of these "reliable" probes. It is important to bear in mind that, especially at larger momentum transfers, the electromagnetic interaction can be significantly clouded by the potential importance of exchange currents.[32]

At higher excitation energy, the $T=0$ normal parity states excited by the K^+ should be compared to the excitation spectrum resulting from α particle inelastic scattering. While the α particle also excites $T=0$ normal parity states, it is not

clear the extent to which such states are predominately p-h or single nucleon excitations. Such comparisons would be useful in determining whether states excited by the α particle are predominantly cluster excitations or p-h.

As a final further example, since $T=0$ normal parity states are expected to dominate the spectrum, one would expect the K^+ to be an ideal probe for investigating the location and spreading of isoscalar giant monopole or quadrupole resonances. Again, if one considers (K^+,K^0), then all $T=0$ states would disappear from the nuclear response. K^+ charge exchange is also an interesting possibility for studies of analog states. We have not actually calculated the appropriate 2^+, $T=0$ spectrum between 10 and 30 MeV excitation in this paper because of difficulties associated with spurious state 2p-2h excitations. Earlier simplified calculations have predicted that 2^+, $T=0$ excitations between 15–22 MeV would be important at medium momentum transfers.

The results of the 300 MeV/c ^{12}C$(K^-,K^{-\prime})^{12}$C* calculations are shown in Fig. 10. The excitation spectrum is very similar to that predicted for $(K^+,K^{+\prime})$ with normal parity 1^- and 3^- states being dominant. In one sense this is fortunate because, as mentioned above, one should understand the nuclear spectroscopy of such states very well from electron and K^+ inelastic scattering. Thus one will be learning about the reaction mechanism from K^- inelastic scattering in this lab momentum range. For example, to what extent is a detailed coupled channels (and Fermi-averaged) treatment of the two-body interaction necessary to correctly predict the inelastic scattering? Once this situation has been clarified, one can use K^- charge exchange to study states not easily seen with other elementary probes. Of course, as for (K^+,K^0) on $T=0$ targets, one can eliminate all $T=0$ excitations by studying $(K^-,\bar{K}^0)$. However, it would be more interesting to study $(K^-,\bar{K}^0)$ on $T\neq 0$ targets. In particular, if one starts with a $T=-T_z$ neutron excess target and uses the $(K^-,\bar{K}^0)$ reaction, then the only final states that can be reached are those states with $T_f=-(T_z+1)$. These isospin stretched states are important for several reasons. For example, one can study the isospin splitting of the $T_>$ and $T_<$ giant dipole resonances as well as that of stretched angular momentum configurations. As a specific case, we consider ^{30}Si$(K^-,\bar{K}^0)^{30}$Al. The results of the calculations for $p_{\text{lab}}^{K^-}=300$ MeV/c are shown in Figs. 11 and 12. By examining Fig. 11, we see that normal parity states completely

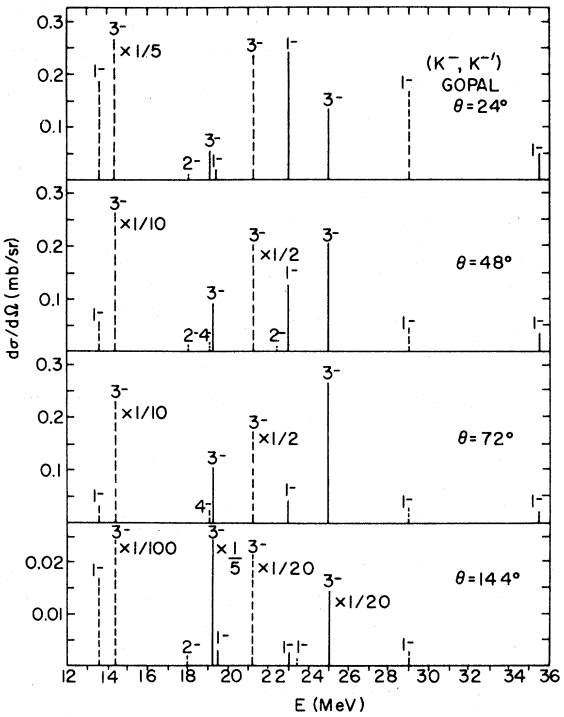

FIG. 10. Differential lab cross sections for K^- inelastic scattering on ^{12}C at $p_{\text{lab}}=300$ MeV/c. The K^-N amplitudes are taken from Gopal *et al.* (Ref. 15). The notation is the same as in Fig. 6.

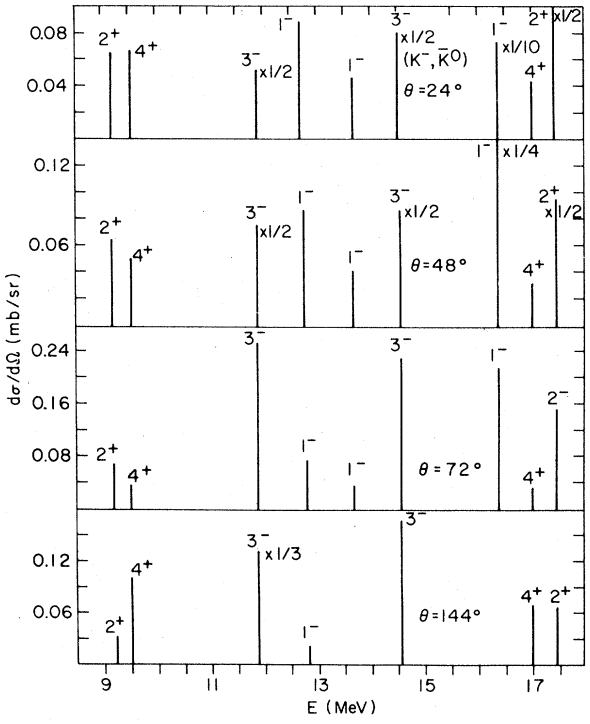

FIG. 11. Differential lab cross sections at selected angles for the charge exchange reaction ^{30}Si$(K^-,\bar{K}^0)^{30}$Al at $p_{\text{lab}}=300$ MeV/c, leading to various diagonalized particle-hole states of ^{30}Al. The notation is the same as in Fig. 6.

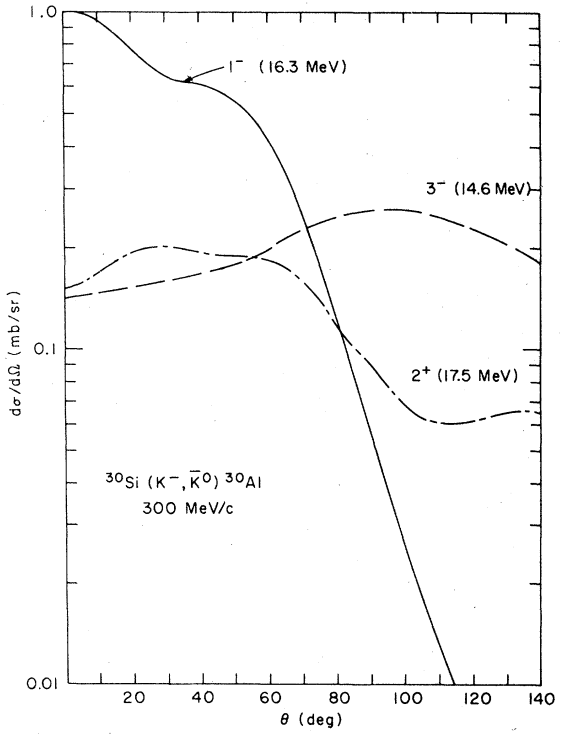

FIG. 12. Angular distributions for the excitation of several of the final states which dominate the ^{30}Si$(K^-,\bar{K}^0)^{30}$Al reaction at 300 MeV/c.

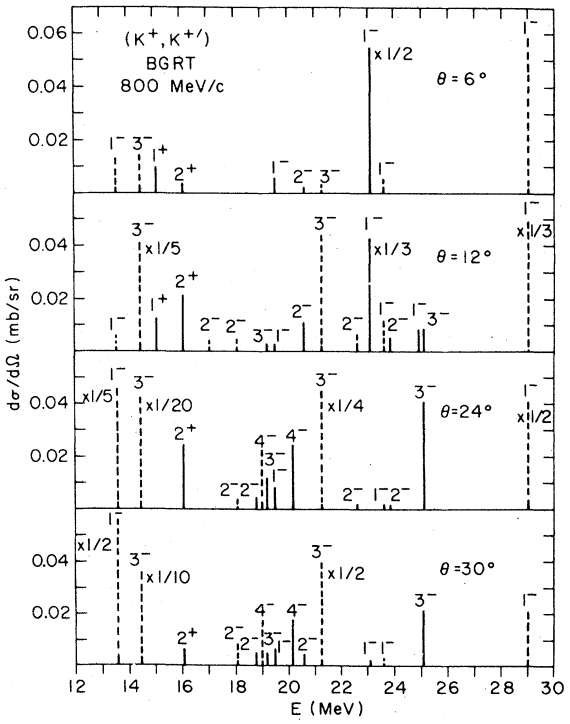

FIG. 13. Differential lab cross sections at selected angles for K^+ inelastic scattering on ^{12}C at 800 MeV/c, using the BGRT$(i)D$ amplitudes of Refs. 13, 14. The notation is the same as in Fig. 6.

dominate the spectrum with high spin states being relatively more important at high momentum transfer as expected. Since the final states all have $T_z = -2$, only $T = 2$ final states are excited. The angular distributions plotted for strongly excited states, shown in Fig. 12, are characteristically different for different spins. When one considers isospin-flip dipole transitions from $T \neq 0$ nuclei, one excites both the $T_>$ and $T_<$ components of the giant dipole resonance. It is of interest to study their splitting as a function of A and Z, and also to determine the degree of concentration of dipole strength. Of course, unless charge exchange is utilized it is difficult to demonstrate that one has actually located the $T_>$ strength. Previously the (n,p) reaction, muon capture,[34] and (π^-,π^0) charge exchange[9] have been suggested as useful experiments for studying the $T_>$ dipole strength. The $(K^-,\bar{K}^0)$ process has an advantage over muon capture in that for the latter reaction one can only study the $T_>$ final state via its decay by nucleon or photon emission. In the case of (π^-,π^0), the difficulties associated with the decay of π^0 into photons makes energy resolution of less than a couple of MeV difficult. Using time of flight techniques one should be able to obtain energy resolution of a few hundred kilovolts in $(K^-,\bar{K}^0)$. Our calculations indicate that approximately 70% of the total $T_>$ dipole strength should be concentrated in the 1^- state strongly excited at 16.3 MeV excitation. Similar studies involving octupole states are also suggested.

There are several ways to construct p-h $T = 1$ states with given spin and single nucleon orbitals that have different parity than the ground state. Of course, if one starts with a $T = 1$, $T_z = -1$ g.s. and goes to a $T = 2$, $T_z = -2$ p-h state, the construction is unique. However, as an example, there are two ways of forming a $T = 1$, $T_z = -1$ p-h state. One could start with a $T = 1$, $T_z = -1$ g.s. such as ^{30}Si and carry out nonisospin-flip inelastic scattering leading to $T = 1$, $T_z = -1$ p-h states. However, another way to construct a $T = 1$, $T_z = -1$ final state would be to start with ^{30}Si and allow for $T' = 1$, $T'_z = 0$ transitions, constructing the final total isospin so that $T_f = T_{zf} = -1$. These different $T_f = 1$, $T_{zf} = -1$ states with identical single nucleon orbital occupation probabilities would have different excitation energies and would have (in the simplest models) relative cross sections given by the ratios $|A/B|^2$ discussed earlier for either K^+ or K^- inelastic scattering. We suggest the study of such states by carrying out inelastic scattering on $T \neq 0$ targets using medium energy kaons.

Before leaving the 300 MeV K^- predictions we

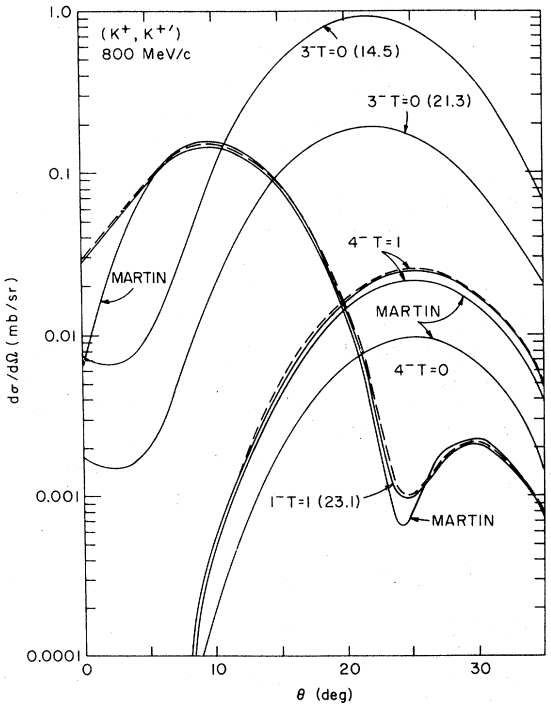

FIG. 14. Angular distributions for K^+ inelastic scattering on ^{12}C at 800 MeV/c. The curves refer to the BGRT(i)D amplitudes of Refs. 13, 14 unless labeled otherwise. The curves for 4$^-$, $T=0$ and 1 refer to the Martin amplitude (Ref. 18), and use $g(p)=1$ for the off-shell form factor; the results for the 1$^-$, $T=1$ state at 23.1 MeV using the Martin amplitude are also shown. The dashed curves use the BGRT(i)D amplitude (13,14), but with $g(p)=1$; the solid curves use the exact $g(p)$. As in Fig. 9 at 300 MeV/c, the cross sections at 800 MeV/c are seen to be only slightly influenced by off-shell extrapolation of the elementary amplitude [$g(p)\neq 1$]. The 4$^-$, $T=0$ curve for amplitude BGRT (i)D is not plotted, but is practically indistinguishable from the 4$^-$, $T=1$ curve shown for BGRT. This should be contrasted with Fig. 8 at 300 MeV/c.

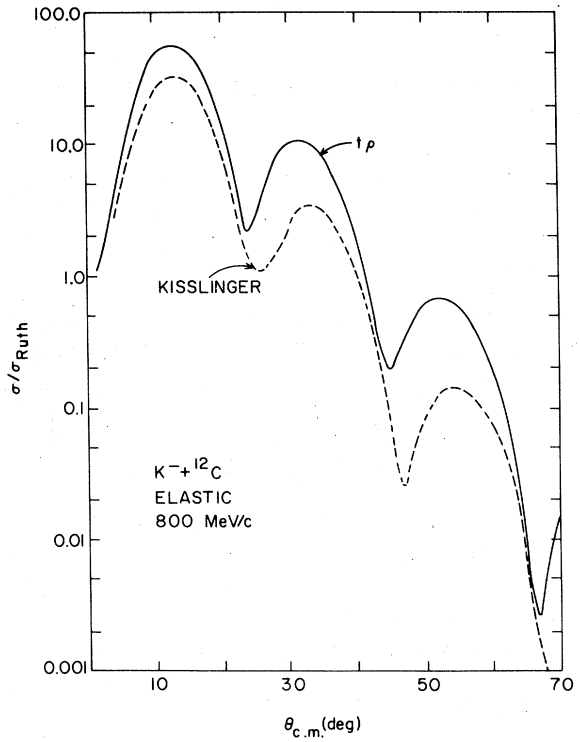

FIG. 15. Elastic scattering differential cross section (divided by Rutherford cross section σ_{Ruth}) for $K^-+^{12}C$ at 800 MeV/c. The solid curve represents the "$t\rho$" approximation of Eq. (29) to the K^- optical potential $V(r)$, including s, p, and d-wave K^-N amplitudes according to Gopal *et al.* (Ref. 15). The dashed curve results from using the Kisslinger form for $V(r)$, as per Eq. (19), with only s and p waves.

note, that as in the case of K^+ inelastic scattering, the dominance of normal parity excited states can be immediately understood from Fig. 5. This figure shows that near 300 MeV/c the term $|A|^2$ dominates for inelastic scattering whereas for charge-exchange (where $A=C=0$) the term $|B|^2$ dominates. Note that the rapid change in the $L=2$ K^- amplitudes near 400 MeV/c [due to the $Y^*(1520)$] make simple predictions for the K^- at low energies more speculative than for the K^+ (in addition to the coupled-channel problems associated with subthreshold open channels).

The first elastic and inelastic scattering experiments planned[35] at the Brookhaven AGS will be for $p_K^{lab}\approx 800$ MeV/c, so predictions in the higher momentum region are particularly timely. In addition, as discussed below, there appears to be less reason to doubt the theoretical predictions at these higher energies, since the elementary amplitudes are better known. The main difficulty encountered by the authors was the computational problem associated with carrying out detailed microscopic calculations employing many partial waves. Significant modifications were required in the code used by Gupta and Walker[9] to study 180 MeV pion inelastic scattering.

Because much of the discussion is similar to that for 300 MeV/c, we proceed to discuss the 800 MeV/c predictions in a somewhat more condensed form.

Figures 3 and 4 indicate that near 800 MeV/c the term $|A|^2$ dominates, so one expects $T=0$ normal parity states to dominate for K^+ inelastic scattering (except in those cases such as $T=1$ dipole and octupole resonances where nuclear structure effects concentrate transition strength). Figure 12 shows the results for the $^{12}C(K^+,K^{+\prime})^{12}C^*$ reaction for 800 MeV/c, demonstrating the prominence of the normal parity states. In addition, the spin-

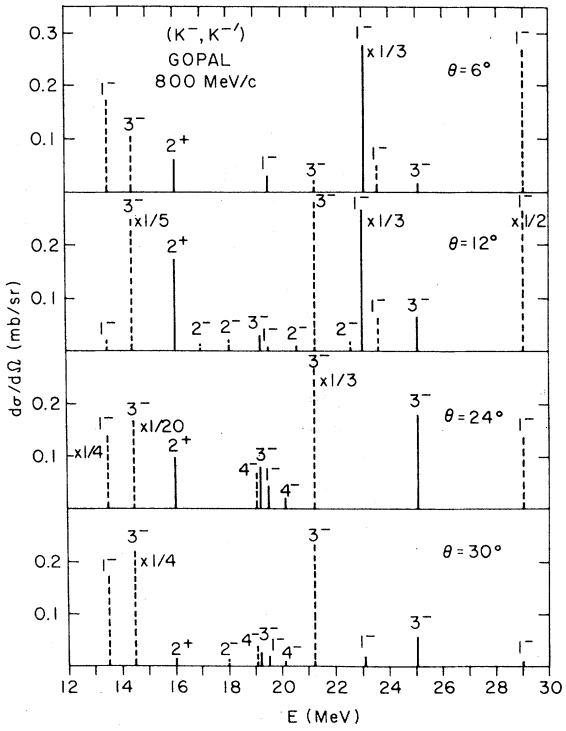

FIG. 16. Differential lab cross sections for K^- inelastic scattering on ^{12}C at 800 MeV/c. We use the K^-N amplitudes of Ref 15. The notation follows that of Fig. 6.

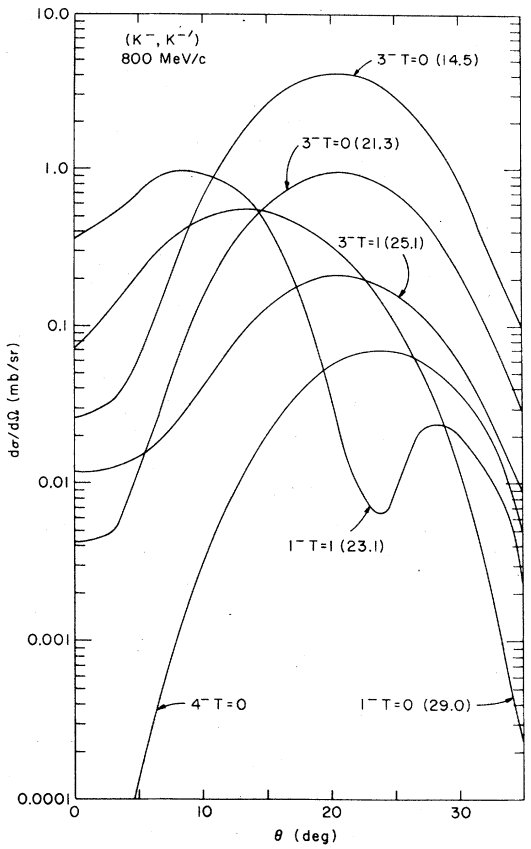

FIG. 17. Angular distributions for K^- inelastic scattering on ^{12}C at 800 MeV/c. We plot the states of each spin which are most strongly excited; the excitation energies are included in parentheses. 2^- states are only weakly excited at this energy.

flip terms $|B|^2$ and $|D|^2$ with Martin and BGRT $(i)D$ amplitudes do not differ nearly as significantly as they do at 300 MeV/c. Hence, one would expect the predictions arising from using the two different amplitudes to be much closer than the dramatic differences shown in Fig. 8. In fact, as illustrated in Fig. 13, the predictions for the angular distributions of selected states are qualitatively similar when using the two sets of elementary amplitudes. Since the same kinds of states are generally predicted to dominate at 800 MeV/c as at 300 MeV/c, we refer the reader to the earlier part of this section for putting K^+ inelastic scattering in perspective with respect to its uniqueness and complementarity in conjunction with other medium energy probes of nuclear structure. As shown in Fig. 14, the effect of setting $g(p)=1$ is negligible, owing to the slow variation of $g(p)$ in momentum space.

In order to calculate K^- inelastic scattering at 800 MeV/c, it is necessary to include $L=2$ K^-N amplitudes in the optical potential for obtaining the distorted waves. In addition, some of the $L=2$ amplitudes are not slowly varying as a function of momentum so that Fermi-averaging of the amplitudes used in the elastic scattering optical potential was performed (as discussed in the previous sections). The difference between including the $L=2$ terms in the simple "ρt" approximation of Eq. (29), and using only the $L=0$ and $L=1$ amplitudes in Eq. (19) is shown in Fig. 15. The difference is seen to be substantial.

The results for the $^{12}C(K^-,K^{-\prime})^{12}C^*$ inelastic scattering at 800 MeV/c are shown in Fig. 16, with characteristic angular distributions for selected strongly excited states shown in Fig. 17. As in the 300 MeV/c case, normal parity states dominate the spectrum. This is expected from examination of the important elementary amplitudes near 800 MeV/c as shown in Fig. 5, where the $|A|^2$ term dominates. We note that for $(K^-,\bar{K}^0)$ charge exchange (where $|A|^2$ and $|C|^2$ are set equal to zero) the $|B|^2$ term dominates and thus one would predict that, qualitatively, normal parity-isospin flip states would completely dominate the spectrum. Thus the 800 MeV/c $K^\pm$-nuclear response function is predicted to be qualitatively very similar to that predicted for 300

MeV/c, with less ambiguity at the higher energies due to uncertainties in the elementary amplitudes.

In conclusion, for kaon inelastic scattering and charge exchange, normal parity states dominate the spectrum with high spin octupole states being relatively more important at high momentum transfer. The K^+ and electron inelastic scattering results should be compared for the same strongly excited states because both are thought to have easily understandable reaction mechanisms (which is the first thing one should check) and thus nuclear wave functions yielding excellent agreement for one probe should also yield high quality results for the other. The K^+ results should also be compared with α particle inelastic scattering as discussed in the text. The K^- inelastic scattering should first be compared with the electron and K^+ results to test the validity of the assumed K^- reaction mechanism. Then the K^- charge exchange appears to be expecially useful for studying the isospin splitting and structure of excited or analog states of $T \neq 0$ nuclei.

Of course, elastic, inelastic, and charge exchange scattering of kaons from nuclei constitute only a modest part of the potential utility of medium energy kaon-nucleus reactions for studying nuclear structure. The present authors feel that deep inelastic (quasieleastic) scattering, (K^+, K^+p) knockout reactions, (K^-, K^+) double strangeness exchange, and the (K^-, π^-) reaction offer other new exciting areas of theoretical and experimental investigation.

One of the authors (G.E.W.) would like to thank the members of the Physics Department at Brookhaven for their hospitality during several extended visits. The reaction calculations reported in this paper were completed on the Brookhaven CDC-7600. This research was supported in part by the Department of Energy under Contract No. EY-76-C-02-0016 and in part by the U. S. National Science Foundation.

[1]A. K. Kerman, H. McManus, and R. M. Thaler, Ann. Phys. (N.Y.) 8, 551 (1959).
[2]C. B. Dover, Proceedings of the Summer Study Meeting on Kaon Physics and Facilities, Brookhaven National Laboratory, June, 1976, Report No. BNL-50579 (available from National Technical Information Service, Springfield, Virginia), p. 9; see also C. B. Dover and P. J. Moffa, Phys. Rev. C 16, 1087 (1977).
[3]G. E. Walker, Bull. Am. Phys. Soc. 21, 646 (1976).
[4]S. R. Cotanch and F. Tabakin, Phys. Rev. C 15, 1379 (1977).
[5]R. D. Koshel, P. J. Moffa, and E. F. Redish, Phys. Rev. Lett. 39, 1319 (1977).
[6]Y. Alexander and P. J. Moffa, Phys. Rev. C 17, 676 (1978).
[7]S. R. Cotanch (unpublished).
[8]C. B. Dover and G. E. Walker, Bull. Am. Phys. Soc. 23, 554 (1978). This is a preliminary report of the results presented here.
[9]M. K. Gupta and G. E. Walker, Nucl. Phys. A256, 444 (1976).
[10]R. Omnes, Nuovo Cimento 8, 316 (1958); M. Gourdin and A. Martin, *ibid.* 8, 699 (1958).
[11]F. Tabakin, Phys. Rev. 177, 1443 (1969).
[12]R. H. Landau and F. Tabakin, Phys. Rev. D 5, 2746 (1972).
[13]G. Giacomelli *et al.*, Nucl. Phys. B71, 138 (1974); we use solution *D* for the isospin zero amplitudes.
[14]G. Giacomelli *et al.*, Nucl. Phys. B20, 301 (1970); we use solution (*i*) for the isospin one amplitudes.
[15]G. P. Gopal *et al.*, Nucl. Phys. B119, 362 (1977).
[16]J. T. Londergan, K. W. McVoy, and E. J. Moniz, Ann. Phys. (N.Y.) 86, 147 (1974).
[17]T. G. Trippe *et al.*, Rev. Mod. Phys. 48, S1 (1976).
[18]B. R. Martin, Nucl. Phys. B94, 413 (1975).
[19]R. H. Landau, S. C. Phatak, and F. Tabakin, Ann. Phys. (N.Y.) 78, 299 (1973).
[20]R. A. Eisenstein and G. A. Miller, PIRK: A computer program to calculate the elastic scattering of pions from nuclei, Carnegie-Mellon Univ., Physics Dept. Report No. CO8-3244-24 (unpublished).
[21]L. S. Kisslinger, Phys. Rev. 98, 761 (1955).
[22]T. W. Donnelly and G. E. Walker, Ann. Phys. (N.Y.) 60, 209 (1970).
[23]P. J. Moffa and G. E. Walker, Nucl. Phys. A222, 140 (1974); A. Picklesimer and G. E. Walker, Phys. Rev. C 17, 237 (1978).
[24]P. M. Endt and C. Van Der Leun, Nucl. Phys. A214, 1 (1973).
[25]B. M. Spicer, Aust. J. Phys. 18, 1 (1965).
[26]L. N. Bolen and J. M. Eisenberg, Phys. Lett. 9, 52 (1964).
[27]T. DeForest, Jr. and J. D. Walecka, Adv. Phys. 15, 1 (1966).
[28]T. W. Donnelly, J. D. Walecka, I. Sick, and G. B. Hughes, Phys. Rev. Lett. 21, 116 (1968); T. W. Donnelly, Phys. Rev. C 1, 833 (1970).
[29]T. S. H. Lee and F. Tabakin, Nucl. Phys. A226, 253 (1974); A. T. Hess and J. M. Eisenberg, Nucl. Phys. A241, 493 (1975).
[30]E. R. Siciliano, private communication.
[31]G. S. Adams *et al.*, Phys. Rev. Lett. 38, 1387 (1977).
[32]M. Chemtob and M. Rho, Nucl. Phys. A163, 1 (1971).
[33]J. T. Londergan, G. Nixon, and G. E. Walker, Indiana University report (unpublished).
[34]B. Goulard, J. Joseph, and F. Ledoyen, Phys. Rev. Lett. 27, 1238 (1971).
[35]P. D. Barnes, R. A. Eisenstein, W. R. Wharton, and E. V. Hungerford, Brookhaven AGS Proposal No. 692, December, 1976, report (unpublished).